Measuring neural coupling from non-Gaussian power spectra of voltage traces taken from awake, behaving animals

B. Masimore, J. Kakalios, A.D. Redish
University of Minnesota, Minneapolis MN 55455

Abstract

Brains consist of complex networks of neurons possessing highly non-linear interactions, suggesting that neural systems will show cooperative dynamics. Previous studies of the non-Gaussian statistics of $1/f$ noise in spin glasses and amorphous semiconductors have revealed important information concerning interaction kinetics not available through other techniques. Five male Brown-Norway-Cross rats were chronically implanted with arrays of microwire electrodes from which local field potentials (LFPs) were recorded from the dorsocentral striatum as the animals performed complex navigational tasks. The power spectra displayed a frequency dependence significantly different from $1/f$. The correlation coefficients of the Fourier transform of the LFPs from striatum showed significant non-zero correlations between frequencies separated by less than three octaves. This novel technique may be useful in measuring functional interactions in neural systems.

Keywords: tetrode, local field potential, neural recording, amorphous silicon, $1/f$ noise, Lorentzian, non-Gaussian

1 Introduction

Neural systems show highly non-linear interactions between their component elements. Delineating these interactions remains a major goal of computational and theoretical neuroscience. In this paper, we borrow analysis techniques from the field of condensed matter physics and apply them to local field potentials recorded from the dorsocentral striatum of awake, behaving rats. These techniques may provide a novel means of measuring and understanding these non-linear interactions.

2 Methods

2.1 Neurophysiological methods

Animals

Five male Brown-Norway Cross rats were used in this study. Rats were obtained from the National Institute on Aging. All procedures were in accordance with NIH guidelines for animal care and were approved by the University of Minnesota IACUC.

The data in this study came from rats trained on two tasks, a navigation task (*the Multiple-T task* [22]) and an operant conditioning task (*the Nose-poke task* [6]). All five of the rats were trained on the navigation task. Four of the rats were also trained on the operant-conditioning task. Data used in this paper are shown in Table 1. During behavioral training, rats received their daily complement of food on the track, while performing behavior. All rats were maintained above 80% of the free-food weight throughout training with additional food if necessary. Rats were handled for 15 minutes per day for three weeks before any training began and then for 15 minutes per day during training, after the animal had run its behavioral session.

The tasks

The Multiple-T task. Details of the Multiple-T task are available elsewhere [21–23]. Briefly, rats were trained to run an elevated loop (mean 4.5 m total distance around the loop) which consisted of three T-shaped choices followed by two return paths. The choice of which return path to take formed a fourth choice. On each return rail, two food pellets

Rat	Age at time of recording	Task		implant-side target
		Multiple-T	Nose-poke	
R010	13–14 mos.	*	*	Right
R011	15 mos.	*	o	Left
R016	10–11 mos.	*	*	Left
R018	14–15 mos.	*	*	Right
R023	13–14 mos.	o	*	Right

Table 1: Experimental details for each rat. For tasks, * indicates data was taken from the animal performing the task in question, o indicates no data was taken from that task,

(Research Diets, New Brunswick NJ) were delivered at each of two sites (four pellets total) by automated food delivery systems (Med-Associates, St. Albans VT). By the time the data were taken that are presented in this paper, the animals were very experienced on this task and ran even novel choice-sequences quickly and efficiently. Rats were run for one 40 minute session per day.

The Nose-poke task. Details of the Nose-poke task are available elsewhere [6]. Briefly, rats were trained to run back and forth along a 1.37 m linear track. At one end of the track was an infra-red LED detector (built in-house); at the other was an automated pellet delivery system (Med-Associates). If the rat blocked the LED continuously for 0.5 sec, a tone sounded. If the rat then ran to the other end of the track, two to four pellets were delivered. If the rat ran to the food-delivery end of the track without blocking the LED for the complete 0.5 sec, no tone sounded and no pellets were delivered. Rats were run for one 40 minute session per day.

Recording details

Local field potentials were recorded from chronically implanted tetrodes using standard techniques. Tetrodes were made from 14 μm NiChrome wire (Kanthal Precision Wire, Palm Coast FL). Tetrodes were loaded into 14-tetrode hyperdrives (David Kopf Instruments, Tujunga CA) allowing each tetrode one-dimension (dorsal/ventral) of individual movement. The hyperdrive was implanted stereotactically (target, Anterior/Posterior, Bregma +0.5 mm, Medial/Lateral, Bregma +3.0 mm). Three animals received right-side implants, two animals received left-side implants (see Table 1). Because no immediately-observable differences were seen between recordings on the two sides [23], we have analyzed the data from all the rats together. Recordings were typically made at a depth of approximately 4.5 mm below Bregma. All electrode locations have been confirmed to lie in the dorsocentral striatum through standard immunohistochemistry techniques.

Surgery was done under general anesthesia under sterile conditions. Rats were first deeply anesthetized with Nembutal (sodium pentobarbital, 40–50 mg/kg) and then placed into the stereotaxic apparatus (David Kopf Instruments). Once on the stereotax, anesthesia was maintained with 0.5–2% isoflurane, vaporized into pure oxygen, delivered at 1.0 L/min. Dual-cillin (Phoenix Pharmaceutical Inc., St. Joseph MO) was used to combat infection (0.1 cc intramuscularly per hind leg). The implant was anchored with 8 jeweler's screws and an additional ground screw was implanted at this time. The ground screw consisted of a jeweler's screw with 0.125 mm insulated stainless-steel wire soldered to it. The steel wire was attached to the hyperdrive through gold-plated Amphenol pins and provided a reliable ground signal for neural recording. A small hole (2 mm diameter) was opened in the skull with a high-speed trephine and the electrodes lowered into place. The implant was then cemented into place with dental acrylic. The dental acrylic forms a permanent, sealed casing around the implant zone, so the skull and brain remain sterile.

After surgery, electrodes were lowered into place over the subsequent two to three weeks.

Local field potentials were recorded with 16 channels of a Cheetah 54-channel system (Neuralynx, Tucson AZ). Signals were amplified at unity-gain at a head-stage (Neuralynx, Tuscon AZ) directly connected to the implant. They were then passed through shielded cables into a 72-channel commutator and then to a pair of Lynx-8 amplifiers ($1\times$–$10{,}000\times$, Neuralynx) and then processed through the Cheetah A2D processor and stored at a sampling frequency of 943 Hz (R010, R011, R016) or 2003 Hz (R018, R023). Signals passing through the Lynx-8 amplifiers were typically amplified $500\times$. All local field potential signals were filtered at 1–475 Hz in the amplifiers.

2.2 Analysis methods

The standard procedure for determining the frequency components of a fluctuating quantity, such as the current passing through a metal or semiconductor, involves Fourier transforming the autocorrelation function of the current [3, 10, 25]. This latter function is defined as the product of the excess current ΔI (that is, the current after the DC average value has been subtracted) passing through the material at a time t and the current at a later time $t+\tau$, averaged over all starting times t. This is given by $\langle \Delta I(t)\Delta I(t+\tau)\rangle$, where the brackets indicate either an ensemble or time average. If fluctuations in the current occur due to some random uncorrelated process, then the auto-correlation function will decrease exponentially [17] as $\langle \Delta I(t)\Delta I(t+\tau)\rangle = \exp(-t/\tau)$. The Fourier transform of this exponentially decaying function will have a Lorentzian frequency dependence, given by $S \sim 4\tau/(1+(\omega\tau)^2)$ where $\omega = 2\pi f$. If the fluctuating quantity is stationary and ergodic over the experimental measurement time, then the two-point auto-correlation function contains all of the relevant information about the fluctuating quantity [18, 19]. The Lorentzian frequency dependence is illustrated in Figure 1, which plots the log of S against the log of the frequency ω. For $\omega\tau \ll 1$, S is approximately constant (that is, frequency independent) while for $\omega\tau \gg 1$, S displays a power law frequency dependence of $S \sim f^{-2}$. It is sometimes convenient to plot the logarithm of the product of the spectral density and the frequency $S \times f$ against the logarithm of the frequency, as shown in Figure 2. In this case, for a Lorentzian function, $Sf \sim f$ for $\omega\tau < 1$ and $Sf \sim f^{-1}$ for $\omega\tau > 1$, with the peak in the plotted function occurring at the corner frequency $\omega \sim 1/\tau$.

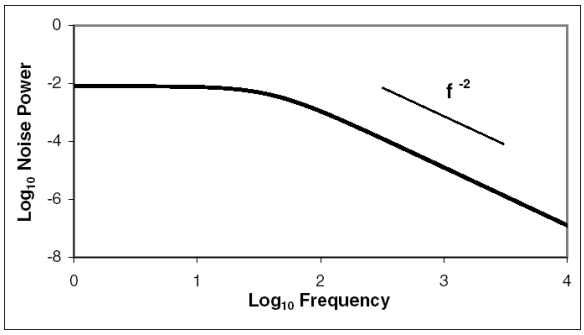

Figure 1: Lorentzian dependence of a single hypothetical fluctuator, plotting the log of S against the log of the frequency ω.

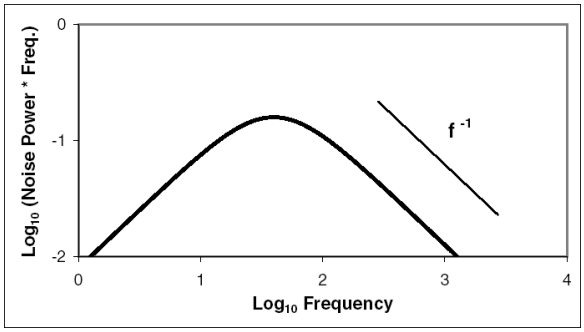

Figure 2: Lorentzian dependence of a single hypothetical fluctuator, plotting the log of $S \times \omega$ against the log of the frequency ω.

Considering the example of an electrical current passing through a semiconductor, one possible physical mechanism underlying the current fluctuations would be scattering of the electrons from a defect, typically an imperfection or impurity in the material. In this case the time τ would be the scattering time, defined as the average time between scattering events, which is proportional to the density of defects in the material. For a system containing two distinct defects having different scattering times, the observed spectral density is the sum of the two distinct Lorentzian spectra, as indicated in Figure 3. In macroscopic, disordered systems, there will be many different defects, each having their own scattering time τ associated with them. The net observed spectral density will therefore be given by the weighted sum of the Lorentzian power spectra

for each defect [10]. If there is a uniform distribution of scattering times $g(\tau)d\tau \sim d\tau/\tau$, then the resulting plot of $\log(S \times f)$ against $\log f$ will be a horizontal line [3], as shown in Figure 4. The data in Figure 4 can be represented by a constant $S \times f$, or equivalently, $S \sim 1/f$. Hence, an ensemble of statistically independent fluctuators, each with their own scattering time τ, will lead to the observation of a spectral density that decays with a power-law frequency dependence. If the scattering times uniformly span the observed frequency range, then there will be no characteristic time describing the resulting spectral density, which is commonly referred to as a $1/f$ spectrum. If the distribution of scattering times is not uniformly distributed over the observed frequency range, so that, for example, the density of high frequency fluctuators is lower than at lower frequencies (equivalently, there are fewer short-time scattering sources), then $S \times f$ will display a decreasing frequency dependence, and the resulting power spectral S will have a power-law spectral slope greater than unity. Such systems, for which the spectral density can be described by an ensemble of a large number of statistically independent fluctuators, are termed Gaussian [10, 18, 19, 27, 28].

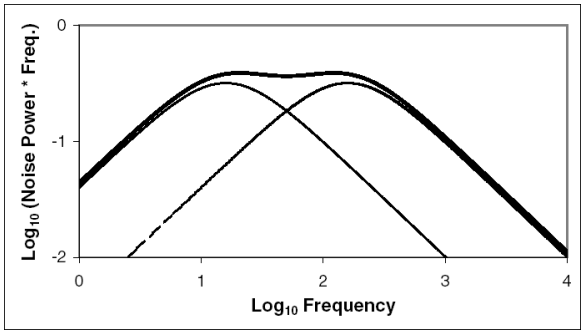

Figure 3: A system containing two hypothetical fluctuators.

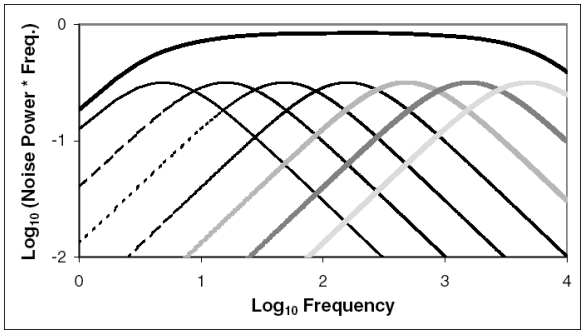

Figure 4: A system containing a uniform distribution of hypothetical fluctuators produces a constant $S \times f$ density.

Figure 5 displays a plot of the voltage signal recorded from an electrode implanted in the striatum of one of the rats described above. This continuous signal can be broken up into a series of voltage recordings, each 0.45 seconds long. A nine second long voltage recording can be therefore considered as twenty successive traces, each 0.45 seconds in duration. The results described in this paper do not depend on the exact length of the time records that the continuous time traces are partitioned into. Figure 6 shows a log-log plot of the Fourier transform of one of the time records in Figure 5. The data in Figure 6 is described by a power-law frequency dependence, that is, $S \sim f^{-\gamma}$, where $\gamma \sim 1.5$. Averaging 1024 distinct Fourier transforms, obtained from an identical number of voltage time records, yields the average power spectrum in Figure 7, also shown on a log-log plot. Comparing the power spectra in Figures 6 and 7 demonstrates that by averaging many spectra together, the contributions of background fluctuations were removed from the main signal of interest from the tetrode.

However, in certain situations, the average spectral density does not contain all of the information regarding the fluctuation phenomena. For example, certain condensed matter systems, such as spin glasses [5, 18, 19, 27, 29] and amorphous semiconductors [7, 15, 16, 20, 24] display fluctuations which are strongly non-Gaussian, that arise from either the number

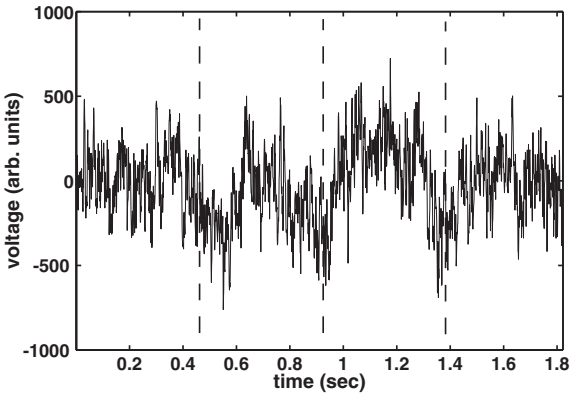

Figure 5: Example voltage signal taken from a single channel of a single tetrode.

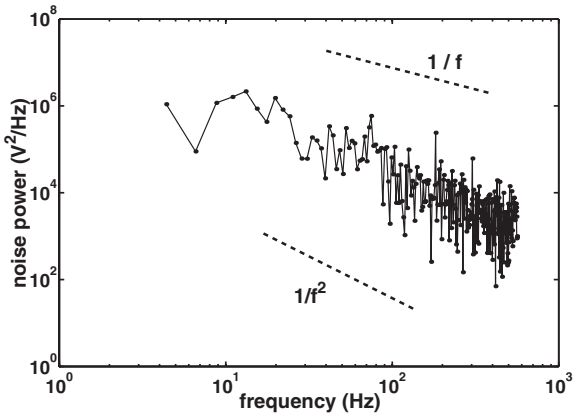

Figure 6: Example single power spectrum taken from a single channel of a single tetrode.

of fluctuators being small (for example, by restricting the sample geometry), or from strong interactions between fluctuators, which has the effect of reducing the number of independent noise sources in a macroscopic sample. These interactions can lead to non-trivial time-dependent variations in the power spectra, so that Fourier transforms of the auto-correlation function at one time can differ from those calculated at a later time. These time dependent fluctuations can be examined by recording a series of Fourier transforms. Since a given time record may contain 1024 current values, its corresponding power spectra will consist of 512 distinct Fourier amplitudes. To monitor any temporal variations in the spectral density, several thousand Fourier transforms may need to be acquired, which quickly results in an unwieldy number of data points. One therefore takes the individual power spectra and sums the noise power into distinct octave bins, as indicated in Figure 7.

All of the spectral density between f_1 and $2f_1$ is integrated, so that a given power spectra is reduced to only seven data points, reflecting the noise power between octaves. (See Table 2 for specific octaves used.) A corresponding plot of the noise power in Figure 7 for octave 2 (8.8–17.6 Hz) and octave 5 (70.2-140.5 Hz) as a function of the number of power spectra successively acquired is shown in Figure 8. These time records of the noise power are not simply random, but contain information about interactions between fluctuators that are not reflected in an average spectral density.

One convenient technique for quantifying the interactions between fluctuators responsible for the variations in the voltage traces is to calculate the correlation coefficient ρ_{ij} defined as the covariance between octave i and octave j normalized by the standard deviation of each octave. That is,

$$\rho_{ij} = \frac{\Sigma(Q_{i,n} - \langle Q_i \rangle)(Q_{j,n} - \langle Q_j \rangle)}{\sigma_i \cdot \sigma_j}$$

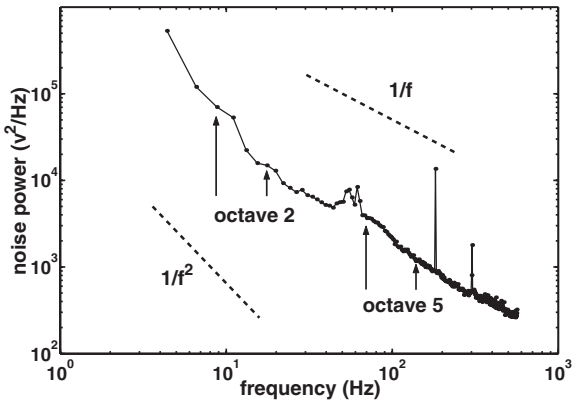

Figure 7: Example average of 1024 power spectra taken from a single channel of a single tetrode, showing how octaves were selected and averaged.

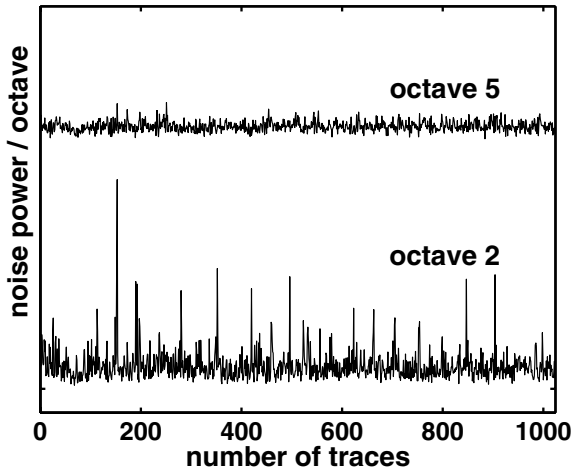

Figure 8: Example noise power at two octaves taken from a single channel of a single tetrode.

where $Q_{i,n}$ is the noise power in octave i for spectrum n, $\langle Q_i \rangle$ is the average noise power in octave i for all N spectra, σ_i is the standard deviation in octave i and the octave indices i and j run from one to seven. The ρ_{ij} vary from +1 to -1, signifying variations from perfectly correlated (+1) to perfectly anticorrelated (-1) behavior. Note that $\rho_{1,1} = 1$ always, since an octave noise power is trivially correlated with itself, while for Gaussian, that is, uncorrelated fluctuations $\rho_{ij} = 0, \forall i \neq j$. Figure 9 shows a plot from Khera & Kakalios [7] of the corresponding average correlation coefficients against octave separation $|i-j|$ for the spectral density of current fluctuations passing through an amorphous semiconductor or through a 5 MΩ carbon resistor. An octave separation of $|i-j| = 3$, for example, indicates that noise power from octave 1 and octave 4 are compared to calculate the correlation coefficient. In Figure 9 all ρ_{ij} values that correspond to a given octave separation are averaged together, and plotted as a single data point. That is, an octave separation of one would include ρ_{ij} between octave 1 and octave 2, octave 2 and octave 3, octave 3 and octave 4, octave 4 and octave 5, and so on being averaged together and expressed as one correlation coefficient number. The current noise in the amorphous semiconductor has an $1/f$ frequency dependence, and is observed to be strongly non-Gaussian, as reflected by the large correlation coefficients in Figure 9. As might be expected, the fluctuations in differing octaves display weaker correlations as the frequency space separation becomes larger. Nevertheless, even for octave separations $|i-j| = 6$, which in this case reflect correlations between an octave at 10-20 Hz and an octave at 750-1500 Hz, the correlation coefficient has a value of 0.2. In contrast, the correlation coefficients for a 5 MΩ resistor are also shown in Figure 9. Here the current noise power spectrum is frequency independent, indicating that temporal variations of the current passing through this resistor are due to uncorrelated thermal

fluctuations [10, 11, 17]. As expected, all $\rho_{ij} = 0$ for any two different octaves, no matter how close or distant in frequency space.

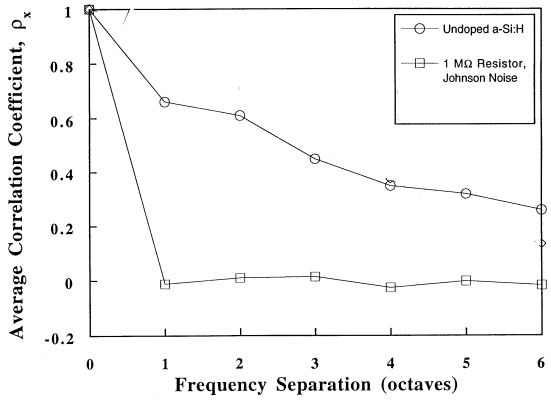

Figure 9: Inter-frequency interactions in amorphous semiconductors (showing non-zero correlations) and in a 5 MΩ resistor (showing Johnson or Thermal noise with no non-zero inter-octave correlations). (After Khera & Kakalios [7].)

2.3 Detailed analysis methods

From each recorded channel 1024 traces of 512 sequential data points were analyzed. Only the data for which the animal was on task were included and any traces for which the signal exceeded the recording threshold were rejected. The first 1024 traces that met both of these criteria were then used. Channels for which 1024 valid traces could not be so constructed were removed. For R018 and R023, each pair of neighboring data points were averaged such that the frequency ranges of all animals are comparable. Each trace was then Fourier transformed as described above and the power spectra summed into octaves as previously described. The details of the octaves are given in Table 2.

Octave number	Frequency Range (Hz) R010, R011, R016	Frequency Range (Hz) R018, R023	Number of FFT Points
1	4.4–8.8	3.9–7.8	2
2	8.8–17.6	7.8–15.6	4
3	17.6–35.1	15.6–31.1	8
4	35.1–70.2	31.1–62.2	16
5	70.2–140.5	62.2–124.4	32
6	140.5–281.0	124.4–248.8	64
7	281.0–562.0	248.8–497.6	128

Table 2: Specific octaves included.

3 Results

The above analysis methods were applied to local field potentials recorded from dorsocentral striatum from five rats running on two complex, behavioral tasks. All records were taken while the rats were awake and active. The first-order power spectra exhibited a power-law frequency dependence, as indicated in Figure 10. All five spectra were consistent with a power-law spectral slope of $f^{-1.2}$ to $f^{-1.6}$ over the frequency range of 10–500 Hz,[1], as summarized in Table 3.

[1]The sharp spikes at 60, 180, and 300, 420, and 540 Hz are due to external 60 cycle signals, not indigenous to the neurophysiology. These do not significantly affect any of the results shown below. All statistics remain unchanged if these spikes are removed from the data.

These slopes were significantly different from $f^{-1.0}$ (ttest, df=5, P<0.05), indicating that the power spectra do not follow a $\frac{1}{f}$ power-law.

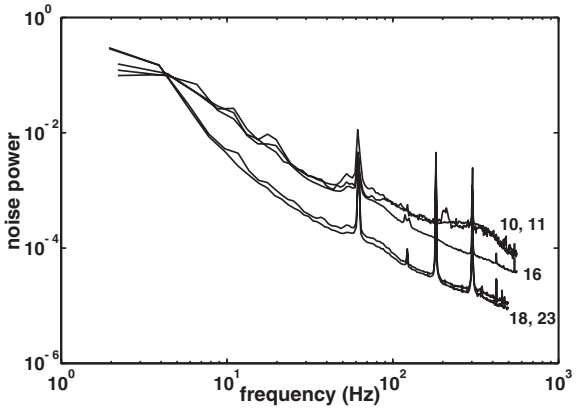

Figure 10: Average power spectra from each animal.

Animal	Mean Slope	95% CI	P(Slope=-1)
R010	-1.37	[-1.33 -1.40]	** P< 0.05, df=38
R011	-1.16	[-1.04 -1.29]	** P< 0.05, df=31
R016	-1.45	[-1.41 -1.50]	** P< 0.05, df=77
R018	-1.46	[-1.34 -1.57]	** P< 0.05, df=35
R023	-1.45	[-1.35 -1.56]	** P< 0.05, df=35
Avg	-1.38	[-1.22 -1.54]	** P< 0.05, df=4

Table 3: For each animal, the mean slope taken over all days is given, along with the 95% confidence intervals. The final column indicates that all five animals had mean slopes significantly different from -1, indicating that none of these spectra followed a $\frac{1}{f}$ power-law. Final row is the average means, taken over the five animals, which is also significantly different from a $\frac{1}{f}$ power-law.

Figure 11 shows the average correlation coefficients across sets of octaves for all five rats, as well as their average (large filled circles). Correlation values between octaves 2 and 3, between 3 and 4, between 4 and 5, etc., are all shown averaged in the one-octave-separation average correlation coefficient. All of the rats showed positive, non-zero average correlations between nearby octaves. Three rats showed average correlations that decayed to zero at large octave separations. Two rats showed average correlations that remained positive even for octave separations of 6 octaves. As noted below, the large average correlation values at large separations for Rats R018 and R023 may be due to experimental artifact. However, the average correlations at small separations (within three octaves) are clearly non-zero (see Table 4).

Separation	Mean	95% CI	P(Separation=0)
1 octave	0.47	[0.3 0.6]	** P<0.05, df=4
2 octaves	0.33	[0.1 0.5]	** P<0.05, df=4
3 octaves	0.23	[0.0 0.5]	** P<0.05, df=4
4 octaves	0.17	[-0.1 0.4]	* P<0.1, df=4
5 octaves	0.14	[-0.1 0.4]	P>0.1, df=4
6 octaves	0.11	[-0.1 0.3]	P>0.1, df=4

Table 4: Correlations across octaves.

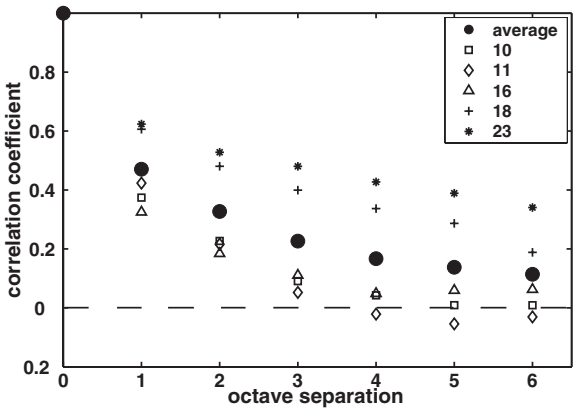

Figure 11: Mean correlations across octaves.

4 Discussion

In this paper, we have presented a novel analysis method which should allow the detection of internal coupling parameters between oscillatory frequencies in neural data. We have shown preliminary data which demonstrates the feasibility of this method.

Local field potentials recorded from dorsocentral striatum showed power-spectra slopes significantly different than 1/f. The decrease in the spectral density with a power-law exponent of 1.5 indicates that in general a lower density of fluctuators operated at frequencies above 100 Hz than was true for lower frequencies. This may arise because local field potentials arise from dendro-synaptic events occurring with generally longer time-courses [14]. Within the local field potential of hippocampus and cortex, oscillation components strong enough to be directly observed are generally seen in the $<$100 Hz range [1, 14, 26]. Specific oscillation components within the striatum have been seen in the theta range (6–10 Hz) [2]. However, the broad peak observed for two rats (R010, R011) may indicate that for these rats there was a large signal that has a characteristic frequency of 200–400 Hz. In rat R010, a clear 200 Hz component was seen. In hippocampus, 200 Hz ripples appear during sharp waves and are associated with key processing states [8].

In dorsocentral striatum, there were significant interactions between frequencies separated by fewer than three octaves. The power law frequency dependence of the spectral density indicates that there are many fluctuating sources contributing to the voltage that is recorded by any given tetrode. This is consistent with the local field potential arising from the summed voltage signals of many different sources [12–14]. The non-zero correlations at short octave separations imply that there are interactions between these multiple signal sources at least at limited spatial ranges.

Whether very large octave separations go to zero or not is still not clear from this preliminary data. Octave separations greater than four octaves were not significantly different from zero. Observing the data, three rats (R010, R011, R016) seem to show zero correlations at long intervals implying a statistical independence of well-separated frequency sources. There were some recording problems with low-frequency-noise rejection in the recordings taken from the other two rats (R018, R023) which could have caused a spurious rise in the overall correlation across all frequency octaves. We therefore believe that any conclusions drawn about the zero or non-zero nature of well-separated octaves will have to wait for future work.

However, the observation that the correlation coefficients are clearly non-zero for octave separations less than three for all rats averaged over all days of testing is in contrast to the correlation coefficients recorded for thermal noise from a 5 MΩ resistor discussed in the Methods section previously. In the case of Johnson or Thermal noise, every fluctuator is statistically independent from all other noise sources, so that even nearest neighbors in frequency space (octave separation of one) show zero correlations. The slower decay to zero of the correlation coefficients observed in the striatal data suggests that there is a finite frequency range, which in turn corresponds to a finite spatial extent, for interactions between sources contributing to the local field potential, but much more work is needed to support this preliminary interpretation.

Because neural processing includes canonical frequencies, it will be important to examine frequency-dependent correlations between specific frequencies rather than just looking at averages across frequency separation as was done here. In addition, it is well known that these canonical frequencies vary with behavioral state. It will thus be important to examine these correlations as a function of behavioral state as well as the task-dependence of these correlations.

Local field potentials filtered with low-pass filters (< 500 Hz) encompass voltages from large regions of neuropil (within 0.5–3 mm of the electrode tip, [12, 14]). However, these analyses can be applied to any continuously recorded voltage traces. It would be very interesting to apply these analyses to multi-unit spike records filtered with higher-frequency band-pass filters (600Hz–6KHz) which encompass voltages from smaller regions of neuropil (within 50–100 μm of the electrode tip, [4, 12, 14]).

All of the correlations reported in this paper are between frequencies recorded at a single location (on a single electrode). In future work, we will examine correlations between signals recorded at different locations. This is similar to the well-studied property of "coherence" [1, 13]. Coherence measures the correlation between oscillations occurring at different spatial locations, thus between different networks of neurons [9]. The method presented here is a generalization of coherence, looking at correlations not just within a single frequency, but also across frequency. This provides additional information about functional coupling at a single location. It will be important to generalize this across-frequency temporal coherence measure to an across-frequency/across-location spatio-temporal coherence measure.

5 Acknowledgements

We thank Jadin Jackson and Neil Schmitzer-Torbert for data collection. We also thank Peter Steinmetz for helpful discussions. We thank T. J. Belich for assistance with the noise analysis. This research was supported by the University of Minnesota (BM, JK, ADR) and by NIH (MH68029-01, ADR). Data collected for this analysis was partially funded by NSF-IGERT training grant #9870633.

References

[1] G. Buzsáki, L. W. Leung, C. H. Vanderwolf (1983) Cellular bases of hippocampal EEG in the behaving rat. *Brain Research* 287(2):139–171.

[2] W. DeCoteau, R. Courtemanche, Y. Kubota, A. Graybiel (2002) Anti-phase theta-range oscillations in striatum and hippocampus recorded in rats during T-maze task performance. *Society for Neuroscience Abstracts* (Program No. 765.6). Online.

[3] P. Dutta, P. M. Horn (1981) Low frequency flucuations in solids: $1/f$ noise. *Rev. Mod. Phys.* 53:497ff.

[4] D. A. Henze, Z. Borhegyi, J. Csicsivari, A. Mamiya, K. D. Harris, G. Buzsaki (2000) Intracellular features predicted by extracellular recordings in the hippocampus *in vivo*. *Journal of Neurophysiology* 84(1):390–400.

[5] N. E. Israeloff, G. B. Alers, M. B. Weissman (1991) Spin fluctuation statistics in CuMn. *Phys. Rev. B* 44:12613ff.

[6] J. C. Jackson, N. C. Schmitzer-Torbert, A. D. Redish (2002) Behavioral correlates of neuronal ensemble in dorsal striatum on a conditioned response task. *Society for Neuroscience Abstracts* Program no. 676.5.

[7] G. M. Khera, J. Kakalios (1997) Temperature and doping dependence of non-Gaussian $1/f$ noise and noise statistics in hydrogenated amorphous silicon. *Phyics Review B* 56:1918–1927.

[8] T. Klausberger, P. J. Magill, L. F. Márton, J. D. B. Roberts, P. M. Cobden, G. Buzsáki, P. Somogyi (2003) Brain-state and cell-type-specific firing of hippocampal interneurons *in vivo*. *Nature* 421:844–848.

[9] B. Kocsis, A. Bragin, G. Buzsaki (1999) Interdependence of multiple theta generators in the hippocampus: a partial coherence analysis. *Journal of Neuroscience* 19(14):6200–6212.

[10] S. Kogan (1996) *Electronic Noise and Fluctuations in Solids*. Cambridge University Press, Cambridge UK.

[11] S. M. Kogan (1985) Low-frequency current noise with a $1/f$ spectrum in solids. *Sov. Phys. Usp.* 28:170ff.

[12] R. Lemon (1984) *Methods for Neuronal Recording in Conscious Animals*. No. 4 in IBRO Handbook Series: Methods in the Neurosciences. Wiley, New York.

[13] D. A. Leopold, Y. Murayama, N. K. Logothetis (2003) Very slow activity fluctuations in monkey visual cortex: Implications for functional brain imaging. *Cerebral Cortex* 13:422–433.

[14] N. Logothetis (2002) The neural basis of the blood-oxygen-level-dependent functional magnetic resonance imaging signal. *Philosophical Transactions of the Royal Society London B* 357:1003–1037.

[15] C. E. Parman, N. E. Israeloff, J. Kakalios (1992) Conductance noise power fluctuations in hydrogenated amorphous silicon. *Physics Review Letters* 69(7):1097–1100.

[16] C. E. Parman, N. E. Israeloff, J. Kakalios (1993) Conductance fluctuations in hydrogenated amorphous silicon. *Phys Rev. B* 47:12578ff.

[17] F. Reif (1965) *Fundamentals of Statistical and Thermal Physics*. McGraw-Hill, New York.

[18] P. J. Restle, R. J. Hamilton, M. B. Weissman, M. S. Love (1985) Tests of Gaussian statistical properties of $1/f$ noise. *Phys. Rev. B* 31:2254ff.

[19] P. J. Restle, M. B. Weissman, G. A. Garfunkle, P. Pearah, H. Morkoc (1986) Non-Gaussian effects in $1/f$ noise in small sillicon-on-sapphire resistors. *Phys. Rev. B* 34:4419ff.

[20] E. V. Russell, N. E. Israeloff (2000) Direct observation of molecular cooperativity near the glass transition. *Nature* 408:695–698.

[21] N. C. Schmitzer-Torbert, J. C. Jackson, A. D. Redish (2002) Behavioral correlates of neuronal activity in the rodent dorsal striatum: The Multiple-t task. *Society for Neuroscience Abstracts* Program no. 676.4.

[22] N. C. Schmitzer-Torbert, A. D. Redish (2002) Development of path stereotypy in a single day in rats on a multiple-t maze. *Archives Italiennes de Biologie* 140:295–301.

[23] N. C. Schmitzer-Torbert, A. D. Redish (Submitted) Neuronal activity in the rodent dorsal striatum on a sequential navigation task: Separation of responses to sequence and reward on the multiple T task .

[24] G. T. Seidler, S. A. Solin, A. C. Marley (1996) Dynamical current redistribution and non-Gaussian $1/f$ noise. *Phys. Rev. Lett.* 76:3049ff.

[25] A. van der Ziel (1979) Flicker noise in electronic devices. *Advances in electronics and electron physics* 49:225ff.

[26] C. H. Vanderwolf (1990) An introduction to the electrical activity of the cerebral cortex: Relations to behavior and control by subcortical inputs. In *The Cerebral Cortex of the Rat*, edited by B. Kolb, R. C. Tees, pp. 151–189. MIT Press, Cambridge MA.

[27] M. B. Weissman (1988) $1/f$ noise and other, slow nonexponential kinetics in condensed matter. *Rev. Mod. Phys.* 60:537ff.

[28] M. B. Weissman (1993) What is a spin glas? A glimpse via mesoscopic noise. *Rev. Mod. Phys.* 65:829ff.

[29] M. B. Weissman, N. E. Israeloff, G. B. Alers (1992) Spin fluctuation statistics: Mesoscopic experiments in CuMn. *Journal of Magnetics and Magnetic Materials* 114:87ff.